APPLICATIONS PAPER

Bundle Block Adjustment of Weakly Connected Aerial Imagery

Yongjun Zhang, Xiaodong Xiong, Xiang Shen, and Zheng Ji

Abstract

In aerial photogrammetry of island and reef areas, traditional aerial triangulation cannot be performed because many images in the block are partially or even completely covered by water, and thus there are not enough tie points among adjacent images. To solve this problem, an effective algorithm of position and orientation system (POS) integrated bundle block adjustment is proposed. The exterior orientation parameters of each image are modeled as functions of corresponding POS observations and their estimated systematic errors. A POS integrated bundle adjustment model is designed with the purpose of effectively eliminating the systematic errors of inertial measurement unit observations. Experimental results of three sets of island aerial images show that the proposed approach can compensate for the systematic errors of POS observations effectively. The topographic mapping requirements of hilly terrain at 1:2 000 scale can be fulfilled, provided that at least one ground control point is used in the bundle adjustment.

Introduction

Obtaining exterior orientation (EO) parameters and ground point coordinates, which is usually accomplished by bundle block adjustment (BBA), is an important procedure in photogrammetry (Brown, 1976; Cramer and Haala, 2010; Zhang *et al*, 2011a). The basic theories and pioneer programs of BBA were well done in the 1965 to 1980 era (Ackermann, 1966; Brown, 1968; Brown, 1976; Case, 1981; Elassal, 1983). In traditional BBA, the ground control points (GCPs) should be measured according to the requirements of national specifications for aerial photogrammetric field work, and then the unknowns (the EO parameters and the object space coordinates of tie and pass points) are calculated by BBA using the GCPs and image tie points. As the BBA model includes nonlinear equations, obtaining proper approximations of the unknowns is essential to the convergence of the computation. In traditional photogrammetry, free network bundle adjustment is performed, and then absolute orientation using the GCPs is conducted to obtain approximations of the unknowns (Zhang *et al.*, 2011b). However, in some unconventional photogrammetric applications, there are large overlap variations and large rotation angles between adjacent images (Zhang *et al.*, 2011b). In these cases, image matching and establishing a free network can be very difficult. This is especially true in island aerial photogrammetry where a great deal of images may be dominantly covered by water. The establishment of a free network usually fails because certain stereo models cannot be successfully connected with each other.

The position and orientation system (POS) is an integration of a global positioning system (GPS) and an inertial measurement unit (IMU), which provides data for the position (i.e., longitude, latitude, and elevation) and the attitude (i.e., the roll, pitch, and yaw angles) of the sensor during the flight mission at small time intervals. The EO parameters of each image can be directly obtained by the integration of POS with an aerial camera. Therefore, POS integrated aerial photography provides two possible solutions for photogrammetric applications: direct georeferencing using POS data and POS integrated BBA (Khoshelham, 2009). Direct georeferencing is usually implemented by forward intersection using the image EO parameters provided by the POS. It is therefore suitable for areas where measuring GCPs is difficult. In the last two decades, intensive research has been conducted for direct georeferencing using POS data (Scaloud *et al.*, 1996; Grejner-Brzezinska, 1999; Cramer *et al.*, 2000; Mostafa and Schwarz, 2001; Yastikli and Jacobsen, 2005; Legat, 2006; Ip *et al.*, 2007; Skaloud and Legat, 2008). At the present stage, great improvements have been obtained in the accuracy of GPS and IMU. However, the POS usually cannot be precisely calibrated before the flight mission. The accuracy of direct georeferencing using POS data obtained by the uncalibrated or roughly calibrated POS still cannot meet the high photogrammetric accuracy demands (Cramer *et al.*, 2000; Yastikli and Jacobsen, 2005; Ip *et al.*, 2007). With the purpose of obtaining precise and reliable results in aerial photogrammetry, POS integrated BBA is one of the best options (Wilkinson *et al.*, 2009). Researchers have shown that the internal accuracy (consistency among images) and the external accuracy (georeferencing accuracy) will be greatly improved after POS integrated BBA even without GCPs (Yastikli and Jacobsen,

The School of Remote Sensing and Information Engineering, Wuhan University, No. 129 Luoyu Road, Wuhan, 430079, P.R. China (zhangyj@whu.edu.cn).

Photogrammetric Engineering & Remote Sensing
Vol. 78, No. 9, September 2012, pp. 000–000.

0099-1112/12/7809–0000/$3.00/0

2005; Ip *et al.*, 2007; Khoshelham, 2009; Zhang *et al.*, 2009). An integrated system of a POS and a digital camera can be used in the surveying and mapping project that only requires moderate accuracy (Zhang *et al.*, 2009; Nagai *et al.*, 2009). However, the POS integrated BBA without GCPs has a limited effect on the elimination of POS systematic errors (Yastikli and Jacobsen, 2005), especially the translation components. If a few GCPs are used in the POS integrated BBA, the systematic errors can be effectively eliminated and the BBA results can meet the requirements of precise topographic mapping. For example, the research of Yuan (2008) shows that POS integrated BBA can achieve precise results that meet the accuracy requirements of topographic mapping with only four full GCPs placed at the corners of the adjustment block for large-scale images of flat regions, and with only one full GCP placed at the center of the adjustment block for medium-small scale images of mountainous regions. For island aerial photogrammetry, the application of POS data solves the problem where the approximations of the EO parameters cannot be obtained through free network bundle adjustment, making the BBA of island aerial images possible. However, a great deal of island aerial images may be partially or even completely covered by water. The connectivity among adjacent images is very weak because there may be not enough tie points. It is also very difficult to measure enough GCPs on these islands because many of them are unreachable. Considering this situation, investigations should be conducted to verify whether the POS integrated BBA of island aerial images can effectively eliminate large systematic errors and that the BBA results can meet the accuracy requirements of precise topographic mapping.

With the purpose of eliminating the systematic errors in the POS integrated BBA, it was necessary to analyze the law of systematic errors and then establish a proper systematic error correction model. The systematic errors of POS observations mainly include the residual GPS antenna offset, the residual IMU boresight misalignment, and the shift and drift errors of GPS/IMU that vary over time. The GPS drift error seemed to be linear in the first approximation for time intervals of up to 15 minutes (Friess and Heuchel, 1992), and the same results were found with the drift error of IMU. The φ-ω-κ rotation angle system defined by sequential rotations about the Y, X, and then Z axis, the ω-φ-κ rotation angle system defined by sequential rotations about the X, Y, and Z axes, and quaternion are generally used by current BBA models to represent the rotation matrices (Yuan, 2008; Hinsken *et al.*, 2004). In this paper, the BBA model was established based on the ω-φ-κ rotation angle system.

Many images may be partially, or even completely, covered by water in island aerial photogrammetry. In this case, the use of POS data is crucial to solving the aerial triangulation problem. The exterior orientation parameters of each image are modeled as functions of the corresponding POS observations and their systematic errors. A POS integrated BBA software was developed to perform the bundle adjustment with aerial images and GCPs from three test fields of island regions. The achieved accuracies with different quantities and distributions of GCPs are further analyzed to verify the correctness and effectiveness of the proposed approach. Finally, the conclusions are discussed.

Mathematical Model of POS Integrated BBA

Exterior Orientation Parameters Represented by POS Observations

Based on the ω-φ-κ rotation angle system, the collinearity equations still have the following general form:

$$\begin{aligned} x - x_0 &= -f\frac{a_1(X-Xs)+b_1(Y-Ys)+c_1(Z-Zs)}{a_3(X-Xs)+b_3(Y-Ys)+c_3(Z-Zs)} \\ y - y_0 &= -f\frac{a_2(X-Xs)+b_2(Y-Ys)+c_2(Z-Zs)}{a_3(X-Xs)+b_3(Y-Ys)+c_3(Z-Zs)} \end{aligned} \quad (1)$$

where x and y are the image plane coordinates of the image point; x_0, y_0, and f are the interior orientation elements; X, Y, and Z are the object space coordinates of the ground point; X_S, Y_S, and Z_S are the object space coordinates of the perspective center, and a_i, b_i, and c_i (i = 1, 2, 3) are the nine elements of the rotation matrix R formed by the three rotation angles ω, φ, and κ.

The GPS antenna cannot be placed at the perspective center of the camera, nor can the axes of the IMU coordinate system be exactly parallel to those of the camera coordinate system. The GPS antenna offset and the IMU boresight misalignment have to be corrected in the POS data postprocessing. Practical experience indicates that some residuals of the GPS antenna offset and IMU boresight misalignment after the postprocessing of POS observations are present. Besides the aforementioned two kinds of residuals, the remaining systematic errors of POS observations are mainly the shift and drift errors.

Within a very short time span (e.g., a few minutes), the random errors of the POS observations are usually very small. These observations can be treated as errorless after compensating for the systematic shift and drift errors. The three islands in this study have less than 20 square kilometers ground coverage. It is therefore practical to calculate the EO parameters using POS observations for island photogrammetry. Considering the characteristics of the GPS and IMU observations, constant and linear items are used to model the systematic errors of POS observations in this paper.

The mathematical model for calculating the perspective center (X_S, Y_S, Z_S) of a specific image with GPS observations (X_G, Y_G, Z_G) can be described as follows:

$$\begin{bmatrix} X_S \\ Y_S \\ Z_S \end{bmatrix} = \begin{bmatrix} X_G \\ Y_G \\ Z_G \end{bmatrix} - R\begin{bmatrix} u \\ v \\ w \end{bmatrix} - \begin{bmatrix} a_X \\ a_Y \\ a_Z \end{bmatrix} - (t - t_0)\begin{bmatrix} b_X \\ b_Y \\ b_Z \end{bmatrix} \quad (2)$$

where (u, v, w) are the remained error of the GPS antenna offset; R is the rotation matrix of the angular elements ω, φ, and κ; (a_X, a_Y, a_Z), and (b_X, b_Y, b_Z), are the systematic offset and drift errors of the GPS observations, respectively; t is the acquisition time of the current image; and t_0 is the reference time, which is usually set as the acquisition time of the central image in each strip.

According to Hinsken *et al.* (2004), the relationship between the IMU observations and the angular EO parameters is $R_{IMU} = R_{MIS}R$, where R_{IMU} is the rotation matrix of the IMU observations ω_I, φ_I, and κ_I; R_{MIS} is the rotation matrix of the boresight misalignment residuals ω_M, φ_M, and κ_M; R is the rotation matrix of the angular elements ω, φ, and κ. $R_{IMU} = R_{MIS}R$ can be easily converted into $R = R_{MIS}^T R_{IMU}$. Considering the strip offset (a_ω, a_φ, a_κ) and drift (b_ω, b_φ, b_κ) of the IMU observations, the mathematic model of calculating the angular elements (ω, φ, κ) of the EO parameters can be described as follows:

$$\begin{bmatrix} \omega \\ \varphi \\ \kappa \end{bmatrix} = \begin{bmatrix} arctg(-b_3/c_3) \\ arcsin(-a_3) \\ arctg(-a_2/a_1) \end{bmatrix} - \begin{bmatrix} a_\omega \\ a_\varphi \\ a_\kappa \end{bmatrix} - (t - t_0)\begin{bmatrix} b_\omega \\ b_\varphi \\ b_\kappa \end{bmatrix} \quad (3)$$

where t and t_0 are the same as that of Equation 2; and a_i, b_i, and c_i (i = 1, 2, 3) are the elements of the production matrix $R_{MIS}^T R_{IMU}$.

Error Equations of Bundle Adjustment

According to the aforementioned systematic error correction model, the unknowns in the POS integrated BBA are the ground point coordinates, the residuals of the GPS antenna offset and IMU boresight misalignment, and the shift and drift errors of the GPS and IMU observations. Equations 2 and 3 should be substituted into Equation 1 to establish the synthetic model of BBA. The error equations of POS integrated BBA can be written as following by mathematical derivation:

$$V_X = Ax + BS_G + CS_I \quad - l, \quad P \tag{4}$$

where V_X is the correction vector of the image points; x is the correction vector of the ground point coordinates; S_G and S_I are the correction vectors of the systematic errors of the GPS and IMU observations; A, B, C are the coefficient matrices of the unknowns; l is the constant vector of the observation equations; and P is the weight matrix of the image points. Here ground control points are treated as errorless. The systematic error of the image points is neglected since the aerial digital camera is precisely calibrated.

If a surveying block includes m flight strips, N images, and n ground points, the number of unknowns of the POS integrated BBA is $3 + 6 \times m + 3 + 6 \times m + 3 \times n$. As can be seen, the number of unknowns is independent of the number of images because the EO parameters are represented as the functions of the GPS and IMU observations. The precise EO parameters are calculated by the GPS and IMU observations and their corresponding systematic errors after bundle adjustment. This strategy is advantageous to overcome the problem caused by weak connections between adjacent images within a short time.

Experiments and Analysis

A POS integrated BBA software to perform bundle adjustment with aerial frame images based on the aforementioned model was developed. With the purpose of verifying the correctness and effectiveness of the proposed POS integrated BBA model, experiments with three sets of island aerial images and GCPs were performed. All aerial images with 0.20 m ground sampling distance (GSD) were obtained with a digital camera UltraCamD by Microsoft; the integrated POS data were obtained with an IGI AeroControl system. The accuracies of the BBA are analyzed to evaluate if they can meet the requirements of topographic mapping at 1:2 000 scale (GB 7930-2008, 2008) in China, as shown in Table 1.

Test field I covers approximately 18 square kilometers and consists of two adjacent islands of hilly terrain, as shown in Figure 1. There are 49 aerial images in four flight strips and 12 GCPs. Six images are completely covered by water, which are automatically discarded during the BBA. Most of the other images are also partially covered by water. A total of 2,177 pass points were automatically obtained by least squares image matching, and the corresponding image points of all 12 GCPs were manually measured.

Direct georeferencing was performed first to calculate the object space coordinates of the GCPs by multi-image forward intersection with the EO parameters directly obtained from POS, and then the residuals of the GCPs were calculated by computing the discrepancies between the measured and computed object space coordinates. The root mean square errors (RMSEs) of the horizontal and vertical residuals are 0.528 m and 1.620 m, respectively; the maximum horizontal and vertical residuals were 0.911 m and

TABLE 1. ACCURACY REQUIREMENTS OF TOPOGRAPHIC MAPPING AT 1:2 000 SCALE IN CHINA

	Maximum Allowed Error (m)			
	Control Point		Checkpoint	
Terrain Types	Horizontal	Vertical	Horizontal	Vertical
Hilly Terrain	0.30	0.26	0.50	0.40
Mountainous Terrain	0.40	0.60	0.70	1.00

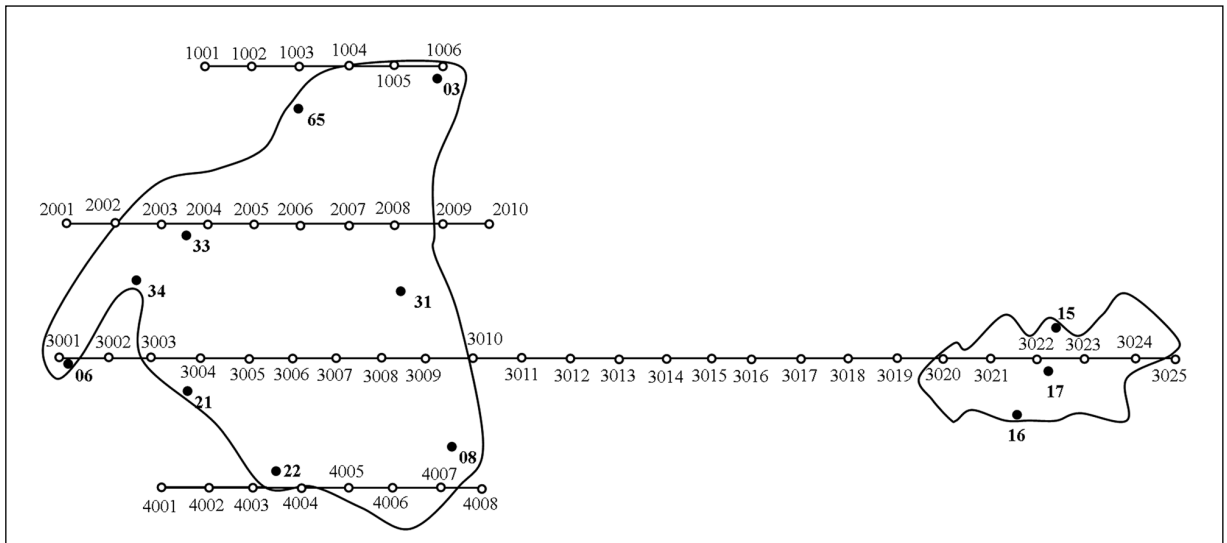

Figure 1. Distribution of images and GCPs of test field I (° the photographic center, • the ground control point).

2.872 m, respectively. These results indicate that the accuracy of direct georeferencing cannot meet the requirements of topographic mapping at 1:2 000 scale.

POS integrated BBAs with zero to four or all of the 12 GCPs were then conducted to evaluate the performance of the proposed approach. Different layout patterns of the GCPs were adopted in the BBA with one to four GCPs. The statistical results of the POS integrated BBA are shown in Table 2. As can be seen, the RMSEs of the horizontal and vertical residuals of the checkpoints are less than 0. 500 m when BBA is performed without GCPs, which indicates that the effectiveness of the BBA in improving the accuracy of georeferencing. Nevertheless, the residual systematic errors are obvious and cannot be neglected due to the absence of GCPs. When one to four GCPs were used in BBA, the RMSEs of the horizontal and vertical residuals of the checkpoints were less than 0.200 m, with the maximum horizontal or vertical residuals less than 0.400 m. The use of all 12 GCPs did not substantially improve the accuracy when compared with those having one to four GCPs, which indicates that stable BBA results can be obtained even with a few GCPs. Moreover, the standard errors of unit weight of all experiments were around 0.0027 mm to 0.0029 mm. The experimental results show that the requirements of topographic mapping of hilly terrain at 1:2 000 scale can be reached when at least one GCP is used in the BBA, regardless of the number and distribution of the GCPs.

Test field II covers about 10 square kilometers and consists of four adjacent islands of hilly terrain, as shown in Figure 2. This test field contains 14 GCPs and 35 aerial images in four flight strips. All the images are partially covered by water. A total of 2,400 pass points were automatically obtained.

The RMSEs of the horizontal and vertical residuals of direct georeferencing are 0.473 m and 2.509 m, respectively. The statistics of the POS integrated BBA with different layout patterns and different numbers of GCPs are shown in Table 3. As can be seen, when the BBA was performed without GCPs, the RMSEs of the horizontal and vertical residuals of the checkpoints were less than 0.500 m. However, the residual systematic errors were also obvious and cannot be neglected due to the absence of GCPs. When one to six GCPs are used, the RMSEs of the horizontal and vertical residuals of the checkpoints were less than 0.275 m and 0.165 m, respectively, and the maximum horizontal and vertical residuals were less than 0.300 m and 0.350 m, respectively. The use of all of the 14 GCPs did not substantially improve the accuracy. The conclusions of this test field are similar to that of the test field I.

As shown in Figure 3, test field III consists of nine small islands of hilly terrain. The total ground coverage of the test field is approximately 15 square kilometers. It contains 16 GCPs and 49 aerial images in five flight strips. All the images are partially or even completely covered by water. A total of 1,756 pass points are automatically matched.

The RMSEs of the horizontal and vertical residuals of direct georeferencing are 0.419 m and 1.884 m, respectively. The results of POS integrated BBAs with different layout patterns and different numbers of GCPs are shown in Table 4. The RMSEs of the horizontal and vertical residuals of the checkpoints are about 0.400 m when the BBA was performed without GCPs. When one to six GCPs were used, the RMSEs of the horizontal and vertical residuals of the checkpoints decreased to about 0.200 m and 0.150 m, respectively; the maximum horizontal and vertical residuals were less than 0.360 m and 0.320 m, respectively. The use of all of the 16 GCPs also had a very limited effect on improving the accuracy. The conclusions of this test field are similar to that of test fields I and II.

It can be seen from the above three experiments that the systematic errors of POS observations can be effectively eliminated and the BBA results can meet the accuracy requirements of topographic mapping of hilly terrain at 1:2 000 scale when only one GCP is used. Moreover, the BBA results are only slightly improved when more GCPs are used, which indicates that the proposed POS integrated BBA model can make full use of the advantages of POS data. Furthermore, the BBA results are independent of the number and distribution of GCPs when at least one GCP is used. At least two GCPs should be used in practical applications, however, to have a backup in case the object coordinates of a GCP are blundered.

TABLE 2. ERROR STATISTICS OF POS INTEGRATED BBA OF TEST FIELD I

Number of GCPs	Names of Used GCPs	Standard Errors of Unit Weight (mm)	GCPs				Checkpoints			
			RMSE of Residuals (m)		Maximum Residuals (m)		RMSE of Residuals (m)		Maximum Residuals (m)	
			Horizontal	Vertical	Horizontal	Vertical	Horizontal	Vertical	Horizontal	Vertical
0	—	0.0029	—	—	—	—	0.440	0.399	0.498	−0.480
1	03	0.0027	0.045	0.252	0.045	−0.252	0.176	0.143	0.265	0.278
	08	0.0028	0.108	0.058	0.108	−0.058	0.144	0.175	0.197	0.348
	15	0.0027	0.022	0.062	0.022	−0.062	0.186	0.187	0.291	0.355
2	06,17	0.0029	0.096	0.074	0.164	−0.075	0.168	0.172	0.252	−0.296
	08,65	0.0027	0.100	0.078	0.106	−0.086	0.191	0.176	0.293	0.347
	15,16	0.0029	0.142	0.134	0.142	−0.137	0.136	0.164	0.203	−0.297
3	03,06,15	0.0027	0.102	0.084	0.155	−0.254	0.158	0.154	0.236	0.285
	08,34,65	0.0028	0.146	0.061	0.194	0.084	0.137	0.195	0.182	0.362
	15,16,31	0.0027	0.135	0.161	0.172	−0.191	0.140	0.165	0.175	−0.301
4	06,16,22,65	0.0029	0.119	0.127	0.195	0.183	0.165	0.195	0.215	−0.347
	15,16,22,31	0.0029	0.122	0.183	0.146	0.233	0.142	0.148	0.179	−0.305
	21,31,33,34	0.0027	0.112	0.152	0.138	−0.209	0.157	0.159	0.215	−0.249
12	All the GCPs	0.0028	0.122	0.158	0.184	−0.249	—	—	—	—

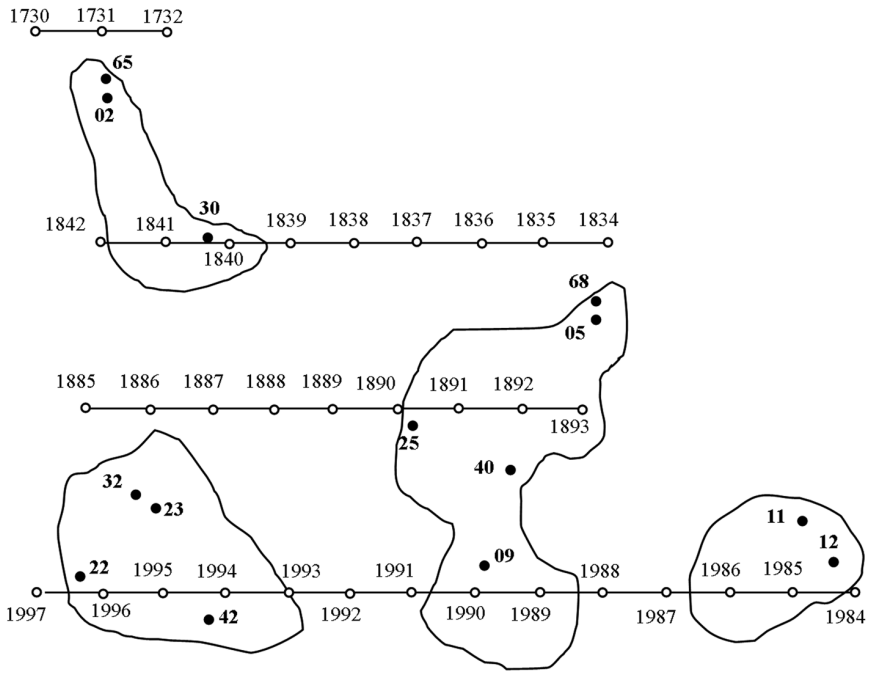

Figure 2. Distribution of images and GCPs of test field II (° the photographic center, • the ground control point).

TABLE 3. ERROR STATISTICS OF POS INTEGRATED BBA OF TEST FIELD II

Number of GCPs	Names of Used GCPs	Standard Errors of Unit Weight (mm)	GCPs				Checkpoints			
			RMSE of Residuals (m)		Maximum Residuals (m)		RMSE of Residuals (m)		Maximum Residuals (m)	
			Horizontal	Vertical	Horizontal	Vertical	Horizontal	Vertical	Horizontal	Vertical
0	—	0.0025	—	—	—	—	0.469	0.304	0.497	0.414
1	30	0.0026	0.208	0.200	0.208	0.200	0.271	0.150	0.297	0.318
	25	0.0025	0.065	0.126	0.065	0.126	0.035	0.101	0.071	0.338
	23	0.0026	0.135	0.057	0.135	0.057	0.116	0.119	0.133	0.313
2	65,09	0.0027	0.184	0.086	0.217	−0.104	0.153	0.107	0.214	0.291
	22,68	0.0026	0.169	0.071	0.172	0.072	0.155	0.134	0.179	0.319
	12,32	0.0026	0.087	0.162	0.105	0.228	0.057	0.057	0.088	−0.142
3	65,12,22	0.0027	0.087	0.144	0.147	−0.239	0.057	0.128	0.148	0.273
	30,68,42	0.0027	0.251	0.181	0.277	−0.216	0.271	0.156	0.298	0.311
	68,30,32	0.0026	0.133	0.128	0.166	0.226	0.160	0.085	0.181	−0.152
4	65,68,12,22	0.0027	0.105	0.104	0.169	−0.192	0.084	0.126	0.170	0.279
	09,22,30,68	0.0027	0.245	0.118	0.266	0.184	0.246	0.162	0.271	0.288
	23,09,68,30	0.0027	0.235	0.106	0.257	0.173	0.233	0.158	0.258	0.281
5	65,68,12,22,25	0.0027	0.087	0.123	0.154	−0.221	0.065	0.129	0.155	0.277
	30,68,11,23,25	0.0027	0.110	0.088	0.134	−0.144	0.108	0.123	0.135	0.280
	30,68,09,22,23	0.0028	0.237	0.121	0.256	0.169	0.229	0.163	0.256	0.258
6	65,68,12,42,23,25	0.0025	0.117	0.130	0.190	−0.210	0.106	0.115	0.189	0.261
	30,68,12,22,09,23	0.0024	0.199	0.107	0.224	−0.152	0.198	0.161	0.222	0.248
	32,25,68,12,09,42	0.0024	0.080	0.142	0.104	0.247	0.101	0.060	0.116	0.097
14	All the GCPs	0.0024	0.033	0.126	0.155	0.229	—	—	—	—

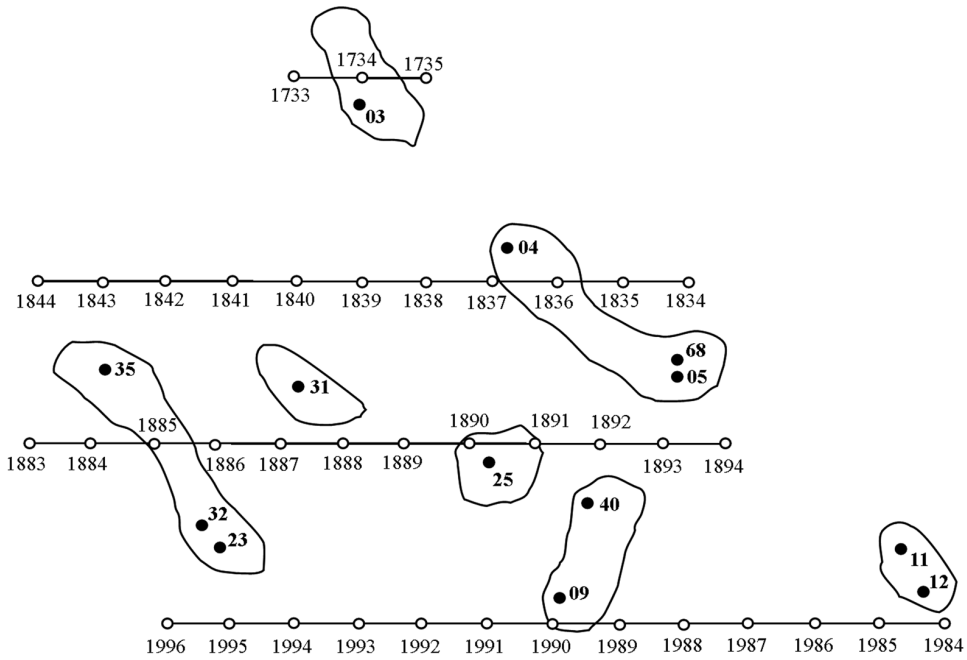

Figure 3. Distribution of images and GCPs of test field III (° the photographic center, • the ground control point).

TABLE 4. ERROR STATISTICS OF POS INTEGRATED BBA OF TEST FIELD III

Number of GCPs	Names of Used GCPs	Standard Errors of Unit Weight (mm)	GCPs				Checkpoints			
			RMSE of Residuals (m)		Maximum Residuals (m)		RMSE of Residuals (m)		Maximum Residuals (m)	
			Horizontal	Vertical	Horizontal	Vertical	Horizontal	Vertical	Horizontal	Vertical
0	—	0.0024	—	—	—	—	0.402	0.332	0.506	0.468
1	23	0.0024	0.118	0.116	0.118	0.116	0.169	0.124	0.356	0.304
	43	0.0024	0.117	0.213	0.117	0.213	0.192	0.112	0.308	0.287
	12	0.0024	0.159	0.121	0.159	0.121	0.175	0.124	0.357	0.300
2	03,27	0.0024	0.115	0.097	0.132	−0.136	0.119	0.123	0.281	0.289
	32,12	0.0024	0.089	0.080	0.098	0.113	0.121	0.124	0.312	0.290
	43,68	0.0024	0.096	0.146	0.113	−0.202	0.128	0.120	0.287	0.299
3	03,12,23	0.0024	0.080	0.125	0.099	−0.148	0.112	0.119	0.315	0.297
	24,35,68	0.0025	0.132	0.155	0.161	0.256	0.134	0.124	0.171	−0.225
	35,04,27	0.0024	0.066	0.014	0.086	−0.019	0.117	0.135	0.286	0.298
4	35,03,12,24	0.0025	0.131	0.157	0.177	0.247	0.114	0.111	0.154	−0.241
	27,24,35,04	0.0025	0.118	0.132	0.187	0.251	0.114	0.127	0.142	−0.221
	12,23,35,04	0.0024	0.060	0.080	0.083	0.111	0.120	0.130	0.313	0.295
5	03,35,12,24,25	0.0025	0.114	0.154	0.201	0.272	0.080	0.110	0.117	−0.221
	35,04,27,43,40	0.0024	0.054	0.096	0.065	−0.196	0.105	0.133	0.267	0.307
	12,43,32,04,09	0.0024	0.054	0.136	0.071	−0.203	0.101	0.111	0.276	0.300
6	03,35,23,12,24,27	0.0024	0.113	0.140	0.204	0.258	0.079	0.107	0.097	−0.224
	35,04,68,23,43,27	0.0024	0.059	0.094	0.070	−0.191	0.108	0.140	0.274	0.313
	43,12,09,23,35,03	0.0024	0.059	0.123	0.081	−0.203	0.099	0.117	0.277	0.301
16	All the GCPs	0.0023	0.054	0.088	0.158	−0.245	—	—	—	—

Conclusions

The integration of POS with an aerial digital camera provides two possible surveying methods for aerial photogrammetry: direct georeferencing and POS integrated BBA. In this paper, both methods were tested using island aerial images with the purpose of verifying whether these two methods are suitable for precise topographic mapping of islands. In order to analyze the systematic errors of the GPS and IMU observations, a POS integrated BBA model based on the ω-φ-κ rotation angle system was adopted to eliminate the systematic errors. The accuracy of direct georeferencing is very limited and cannot fulfill the accuracy requirements of topographic mapping at 1:2 000 scale. However, POS integrated BBA without GCPs can improve the accuracy of georeferencing remarkably, although the systematic errors cannot be eliminated. If one GCP at any location is used in the POS integrated BBA, the systematic errors can be effectively eliminated and the accuracy requirements of topographic mapping of hilly terrain at 1:2 000 scale can be reached, which verifies the correctness and effectiveness of the proposed approach. However, according to reliability theory, the BBA results will be more reliable and the possible outliers of the POS data and GCPs can be found and removed when at least one GCP is used. Two GCPs are recommended, though, in practical applications of aerial triangulation of island aerial images.

The suitability of the proposed approach for aerial images of large islands (e.g., larger than 100 square kilometers) needs to be further investigated. It is conceivable that the POS integrated BBA with the EO parameters as unknowns could be used to deal with the random errors of POS observations since it is possible to measure an ample number of GCPs on a large island.

Acknowledgments

This work was supported by the National Natural Science Foundation of China with Project No. 41171292 and 41071233, the National Key Technology Research and Development Program with Project No. 2011BAH12B05, and the National High Technology Research and Development Program with Project No. 2009AA121403. We are very grateful also for the comments and contributions of anonymous reviewers and members of the editorial team.

References

Ackermann, F.E., 1966. On the theoretical accuracy of planimetric block triangulation, *Photgrammetria*, 21(5):145–170.

Brown, D.C., 1968. Inversion of very large matrices encountered in large scale problems of photogrammetry and photographic astrometry, *Proceedings of the Conference of Photographic Astrometric Technique*, University of South Florida, Tampa, Florida, p.249–263.

Brown, D.C., 1976. The bundle adjustment - Progress and prospects, *International Archives of Photogrammetry*, 21(3), Paper number 3-03, 33 pages.

Case, J.B., 1981. Automation in photogrammetry, *Photogrammetric Engineering & Remote Sensing*, 47(3):335–341.

Cramer, M., D. Stallmann, and N. Haala, 2000. Direct georeferencing using GPS/inertial exterior orientations for photogrammetric applications, *International Archives of Photogrammetry, Remote Sensing and Spatial Information Sciences*, 33(B3):198–205.

Cramer, M., and N. Haala, 2010. DGPF project: Evaluation of digital photogrammetric aerial-based imaging systems - Overview and results from the pilot center, *Photogrammetric Engineering & Remote Sensing*, 76(9):1019–1029.

Elassal, A.A., 1983. Generalized adjustment by least squares (GALS), *Photogrammetric Engineering & Remote Sensing*, 49(2):201–206.

Friess, P., and T. Heuchel, 1992. Experience with GPS-supported aerial triangulation, *International Archives of Photogrammetry, Remote Sensing and Spatial Information Sciences*, 29(1): 299–305.

GB 7930-2008, 2008. *Specifications for Aerophotogrammetric Office Operation 1:500 1:1000 1:2000 Topographical Maps*, Standards Press of China, Beijing, China, 7 p.

Grejner-Brzezinska, D.A., 1999. Direct exterior orientation of airborne imagery with GPS/INS system: Performance analysis, *Navigation*, 46(4):261–270.

Hinsken, L., S. Miller, U. Tempelmann, R. Uebbing, and S. Walker, 2004. Triangulation of LH systems' ADS40 imagery using ORIMA GPS/IMU, *International Archives of Photogrammetry, Remote Sensing and Spatial Information Sciences*, 34(B3): 156–162.

Ip, A., N. El-Sheimy, and M. Mostafa, 2007. Performance analysis of integrated sensor orientation, *Photogrammetric Engineering & Remote Sensing*, 73(1):89–97.

Khoshelham, K, 2009. Role of tie points in integrated sensor orientation for photogrammetric map compilation, *Photogrammetric Engineering & Remote Sensing*, 75(3):305–311.

Legat, K., 2006. Approximate direct georeferencing in national coordinates, *ISPRS Journal of Photogrammetry and Remote Sensing*, 60(4):239–255.

Mostafa, M.M.R., and K.P. Schwarz, 2001. Digital image georeferencing from a multiple camera system by GPS/INS, *ISPRS Journal of Photogrammetry and Remote Sensing*, 56(1):1–12.

Nagai, M., T. Chen, R. Shibasaki, H. Kumagai, and A. Ahmed, 2009. UAV-borne 3-D mapping system by multisensor integration, *IEEE Transactions on Geoscience and Remote Sensing*, 47(3): 701–708.

Scaloud, J., M. Cramer, and K.P. Schwarz, 1996. Exterior orientation by direct measurement of camera position and attitude, *International Archives of Photogrammetry, Remote Sensing and Spatial Information Sciences*, 31(B3):125–130.

Skaloud, J., and K. Legat, 2008. Theory and reality of direct georeferencing in national coordinates, *ISPRS Journal of Photogrammetry and Remote Sensing*, 63(2):272–282.

Wilkinson, B.E., B.A. Dewitt, A.C. Watts, A.H. Mohamed, and M.A. Burgess, 2009. A new approach for pass-point generation from aerial video imagery, *Photogrammetric Engineering & Remote Sensing*, 75(12):1415–1423.

Yastikli, N., and K. Jacobsen, 2005. Direct sensor orientation for large scale mapping – Potential, problems, solutions, *The Photogrammetric Record*, 20(111):274–284.

Yuan, X.X., 2008. A novel method of systematic error compensation for a position and orientation system, *Progress in Natural Science*, 18:953–963.

Zhang, Y.J., Z.X. Zhang, M.S. Sun, and T. Ke, 2011a. Precise orthoimage generation of Dunhuang wall painting, *Photogrammetric Engineering & Remote Sensing*, 77(6):631–640.

Zhang, Y.J., J.X. Xiong, and L.J. Hao, 2011b. Photogrammetric processing of low-altitude images acquired by unpiloted aerial vehicles, *The Photogrammetric Record*, 26(134):190–211.

Zhang, Z.X., Y.J. Zhang, T. Ke, and D.H. Guo, 2009. Photogrammetry for first response in Wenchuan earthquake, *Photogrammetric Engineering & Remote Sensing*, 75(5):510–513.

(Received 26 September 2010; accepted 12 December 2011; final version 21 January 2012)